127654

AEROPROJECTS INCORPORATED
WEST CHESTER, PENNSYLVANIA

FUNDAMENTALS OF ULTRASONIC WELDING

PHASE II

Bimonthly Progress Report No. 6

December 30, 1959

Prepared under

Contract NOas 59-6070-c

Submitted to

Bureau of Naval Weapons

AEROPROJECTS INCORPORATED

WEST CHESTER, PENNSYLVANIA

FUNDAMENTALS OF ULTRASONIC WELDING

PHASE II

December 30, 1959

Prepared under

Contract NOas 59-6070-c

Submitted to

Bureau of Naval Weapons

Bimonthly Progress Report No. 6

October 16 to December 15, 1959

The information contained in this progress report is preliminary and subject to correction and revision

AEROPROJECTS INCORPORATED
West Chester, Pennsylvania

ABSTRACT

Investigation of the relationship of various material properties to weldability indicates that ultrasonic weldability, at least in part, depends upon room temperature hardness.

Further study of the threshold curve substantiates previous tentative conclusions that the minimum power locale in the curve is associated with the best impedance match between the transducer and the weld.

An autoradiographic technique has been developed and applied to the inspection of oxide distribution at the weld interface. Surface film fragments can be distinguished from voids. Oxide thicknesses in the range of 500-3000 angstroms have a significant effect on weld strength and welding parameters.

A positive-replica technique was used in an electron microscopic study of ultrasonically welded iron and copper monometal specimens. Characteristics of the interfacial mechanics and metallurgy were recorded.

TABLE OF CONTENTS

LIST OF TABLES

LIST OF FIGURES

LIST OF FIGURES (Concluded)

I. INTRODUCTION

Research has continued under Phase II of this program to develop a phenomenological theory of ultrasonic welding that will account for the observed effects and that can also be used to improve the design of the equipment and to extend its usefulness in the newer, high-temperature, corrosion-resistant materials of significance to military and atomic energy programs.

Results of our investigation to determine the relationship of various material properties to weldability were reviewed and analyzed. The significance of the threshold curves showing the relationship between minimum power required to weld and clamping force was further investigated.

The influence of surface oxide films on weldability has been studied with anodized coatings of various thicknesses on aluminum. A factorial experiment indicated significant interaction between the thickness of the oxide film, the welding parameters, and the bond strength. Additional work will be required to evaluate the interrelation among those factors.

Examination of the interfacial oxide distribution has been augmented by autoradiography. The anodized surfaces were impregnated with a radioactive tracer (Ni^{63}) before welding. Differences in the metallographic and autoradiographic structures are indicative of the behavior of the surface films and characteristics of the weld interface. Since the resolution of optical microscopy is limited, the fine structural details of the interface require examination by electron metallography.

Preliminary electron microscopic examination of the ultrasonic iron and copper monowelds appears to support conclusions reached in the photoelastic studies.

II. RELATIONSHIP OF MATERIAL PROPERTIES TO WELDABILITY

A. Hardness

The investigation to determine the relationship of various material properties to weldability has been a continuing part of this program*. Determinable properties were tabulated in an effort to delineate obvious first-order effects as each subject material was welded.

Figure 1 is a plot of the total input of vibratory energy required to make a weld as a function of Vickers hardness with parameters of gage. Figure 2 is a plot of acoustical energy per unit weld area as a function of Vickers hardness with parameters of gage. Figure 3 shows the relationship between acoustical energy and gage with parameters of Vickers hardness.

Figure 1 shows that more energy is required to form a weld as gage and hardness increase, but the influence of hardness appears to reach a limit.

Figure 2 shows that the energy per unit weld area required to generate a weld increases with both gage and hardness, and no limiting condition is indicated. Review of weld area data indicates a nonlinear area decrease with hardness. This accounts for the limiting conditions noted in Figure 1. Figure 3 indicates the significance of room temperature hardness on weldability.

B. Significance of the Threshold Curve

The investigation to determine the precise significance of the threshold curve of minimum power required versus clamping force to effect a successful weld, was described in Progress Report No. 5, which also contained preliminary results. Additional information which substantiates the previously drawn conclusions is presented here and essentially completes this study insofar as Phase II is concerned.

As previously outlined (Progress Report No. 5) the independent variables chosen for this investigation were input electrical power applied for a predetermined time, and clamping force with a predetermined sonotrode tip radius. The region of investigations for these independent variables surrounds the locale previously established as representing the "minimum energy condition", namely, the clamping force and input power at which minimum energy is required to produce a weld that will fail by "nugget pullout" in a "peel" test.

---

* Sect. IIC of Progress Report 1 and Sect. IIB of Progress Report 5 on this contract.

The dependent variables observed have been tensile-shear strength, cross-tension strength, weld area, thickness deformation, and temperature. A series of determinations of these dependent variables has been completed for each of several materials. The results of these measurements are recorded graphically in this progress report and extend the information previously reported.

Temperature data were obtained at only six points for the copper because of the limited time remaining. The temperature data were not obtained for the stainless steel because of the difficulty of getting consistently good temperature records with the very thin material.

1. Description and Discussion of Data

Figures 4 through 19 present data obtained from the measurement of monometal welds of 0.005-in. cold rolled and 0.010-in. annealed 302 stainless steel; and 0.020-in. copper in the half-hard condition. These data follow the pattern established in Progress Report No. 5.

Figures 4, 9, and 14 show the threshold curves for these materials. These threshold curves were used as guides in designing the remainder of the experiments.

Figures 5, 10, and 15 are surface plots showing the tensile-shear strength associated with various levels of clamping force and power. In all figures, the area solidly outlined represents the region of minimum power at which successful welding occurred and the associated optimum clamping force (hereafter referred to as the minimum energy condition, MEC) in the threshold curve. These figures show that the highest tensile-shear strength occurs at higher power and clamping force than those of the MEC. In this they are consistent with data obtained for aluminum.

Figure 5 shows a complete foldover in the surface plot. Metallographic examination of specimens obtained in the power range of this foldover indicated that excess power was used even at these reasonably short welding times, resulting in an unsatisfactory weld due to either cracking or surface damage. Thus, best shear strength was obtained at a power and clamping force but slightly greater than the MEC.

Figure 10, for the 0.010-in. stainless steel, shows that the tensile-shear strength falls rapidly when the clamping force rises to a level beyond the range of the threshold curve (about 350 lb). This fall-off is tentatively ascribed to a large increase in area with a concommitant reduction in available power per unit weld area. The data of Figure 12 reveals the increase in area which probably resulted from the annealed condition of the material.

Figure 15 for the copper, shows a similar reduction in strength at clamping forces outside of the established threshold curve. A study of

the associated area data in Figure 17 indicates again a result similar to that obtained for the 0.010-in. stainless steel.

Figures 6, 11, and 16 show curves of the cross-tension strengths for the 0.005-in. stainless steel, the 0.010-in. stainless steel, and the 0.020-in. half-hard copper. The cross-tension strength did not decrease in the same way as did the tensile-shear strength. These experiments were run with the tensile- and cross-tension specimens randomly made, and no simple explanation for this situation is yet evident.

Figures 7, 12, and 17 show the effect of power and clamping force on weld area. For aluminum (Progress Report 5), the weld area becomes larger with increasing power and clamping force and further indicates that the increasing area partially accounts for the higher values of tensile- and cross-tension strength associated with higher power and clamping force. This appears true when these powers and clamping forces do not greatly exceed the MEC values.

The deformation data appear in Figures 8, 13, and 18. In the region of low power and high clamping force, deformation is limited at all clamping force levels; increasing power increases deformation except at the highest clamping forces. The effect of increased clamping force levels is to increase deformation except at the low power levels.

Metallographic examination of specimens surrounding the threshold curve substantiates the graphical data. Low quality welds were obtained in regions far removed from the threshold curve. High clamping forces and low power resulted in poor joints, while excessive power even at the reasonably short welding time of 1 sec at all clamping forces usually resulted in cracks in and around the weld zone.

The temperature data tabulated in Figure 19 follows the same trend as presented in Figures 6 and 10 of Progress Report 5. For example, at any specific power level in the vicinity of the MEC the temperature maximizes at the clamping force level of the MEC. As stated in Progress Report 5 this is the only variable that appears to be clearly related to the MEC.

2. Discussion and Conclusions

Tensile-shear strength, cross-tension strength, weld area, and deformation are related to the minimum energy condition only in a general way, that is, the maxima for each of these occurs at powers and clamping forces greater than the MEC. These are related to the threshold curve in that inferior welds result at excessive power or at clamping forces substantially greater than the optimum.

The temperature data however indicates that, at any fixed power level, the maximum temperature during welding occurs at the clamping force associated with the MEC.

Hence, it is concluded that the threshold curve, and in particular the MEC, is related to the efficiency of energy delivery into the weld being made, and is not critically related to the mechanical properties of the resulting weld. The clamping force affects the coupling of the transducer to the weldment and, thus has a controlling influence on the impedance match between the sonotrode and the weld.

III. EXAMINATION OF WELDMENTS BY AUTORADIOGRAPHIC TECHNIQUES

Studies of the ultrasonic bonding phenomenon during this investigation have been concerned with considerations of transient elastic stress distributions, the energetics of the transducer-weldment-configuration, and the influences of material properties. Surface barrier films and scales have not been considered in any of these studies, but their significance cannot be overlooked since bonding is initiated at the faying surfaces, and interference by foreign materials may have a significant effect on the formation and characteristics of the bond.

Experience has indicated that surface films are an important factor in the bonding process. Some materials as exemplified by certain aluminums and Inconel X appear to develop greater bond strengths when welded with the mill-finish coating intact. Chemical cleaning procedures which effectively remove the film decrease the bond strength, but surface roughness is affected thereby. The features of the bond interface for the mill-finish and chemically cleaned materials are characteristically different. Turbulence, film fragmentation and dispersion, and interpenetration of the faying surfaces occur when surfaces have not been prepared. Chemically prepared surfaces result in a bond of negligible interpenetration; the bond line is intermittently interrupted in continuity but experiences little dispersion.

The heat-treated aluminum alloys, with oxide films formed at elevated temperatures, are generally difficult to bond without prior removal of the adherent scale. In this case, somewhat more effective surface preparation is achieved by mechanical methods than by chemical treatments. The reasons for difficulty in bonding through this heat-treat scale are not fully understood, but probably are a result of the combined thickness and composition of the oxide.

Figure 20 shows that bonding can be achieved through heat-treat scales. These photomicrographs were made of welds in equivalent gages of Inconel X with the oxide intact (a) and with the oxide removed by chemical deoxidizing (b) prior to welding. The differences in the microstructural characteristics are evident. In this instance, unlike aluminum, the surface scale is loosely adherent and supported by a very hard substrate. It is evident that removal of the scale before welding seems to have induced less energy dissipation at the interface whereas the presence of the scale localized energy degradation around the interface. This seems not to be in contradiction with experience involving the use of foil interleaf to augment welding of heavy gage or hard aluminum alloys, titanium alloys, and certain bimetal combinations. Moreover, it supports previous comments concerning chemical cleaning compared to mechanical abrasion.

In an effort to consider the effect of surface films on weldability and the eventual distribution thereof after the completion of the weld cycle, an experiment was designed in which anodized coatings were used as the film. This material was chosen for several reasons: (1) aluminum and aluminum alloys have been investigated most extensively in

previous work, (2) the coatings were readily obtainable in several thicknesses, (3) the porous anodized coatings were amenable to radioactive-tracer impregnation, and (4) welding parameters for this material were within the range of capability of the instrumented 2000-watt research welder. Several disadvantages of using the anodized aluminum surfaces are: (1) the high adhesion between anodized films and aluminum, and (2) the large difference in hardness of the oxide and base metal, which restricts generalizations from the results obtained; however, these were not regarded as sufficient to favor an alternative metal-oxide system.

Preliminary results of this experiment have been reported in Progress Report No. 5. Statistical evaluation of the results of the strength (tension-shear) tests (Tables I and II) indicate a significant difference in weld strength due to different welding parameters and different thicknesses of oxide coating. The standard deviation of tensile-shear strength measurements for the entire experiment is 10.75 lb, which is a measure of the consistency of the ultrasonic welds within the limitations of this experiment.

Specimens were impregnated with the radioactive tracer by treatment in a nickel acetate solution containing a small quantity of Ni^{63}. Good absorption of the tracer was obtained within 1/2 hr at 200°F. This surface treatment was observed to have an adverse influence on the weldability of the test pieces. Several specimens failed to bond at the selected welding machine settings; the control specimens (treated only in boiling distilled water to seal the film) were bonded without difficulty.

Metallographic examination of the radioactive samples indicated that bonding was achieved only in the peripheral region of the weld spot*. The central portion of the weld area contained unbonded areas. The bonding which occurred in the peripheral region, however, was quite adequate to carry out the autoradiographic investigation of the interface.

The Kodak Permeable Base Autoradiographic Stripping Film (experimental) technique described in the Final Report ("Fundamentals of Ultrasonic Welding", Contract NOas 58-108-c), was used in the preparation of the specimens. Exposures were carried out for 120 hr at each oxide thickness level (500, 1000 and 3000 Å), and all specimens were processed simultaneously to reduce processing variables. This technique permits optical examination of the autoradiographic replica in situ on the specimen surface. All specimens were sectioned normal to the weld interface for metallographic examination.

Several interesting results were obtained from this study. The autoradiographic image faithfully delineates the oxide film distribution along the weld interface and distinguishes discrete oxide particles or agglomerates from small voids which are produced in regions of high plastic

* Pages 14-15, Progress Report 3.

turbulence. These voids are quite difficult to resolve under bright-field illumination and can be identified only in the actual specimen by polarized light methods. The voids characteristically occur in those regions where the fragmented oxide particles "bridge" or restrain the material from making contact. Close examination also reveals that some material identified as oxide in the microstructure cannot be observed on the autoradiograph replica. It has tentatively been concluded that oxide generated during the bonding process will satisfactorily explain this because it would not be radioactive.

The two photomicrographs of Figure 21 (a and b) illustrate the observations described: (a) the structure along the interface in a peripheral bond region with shadows resulting from focussing through the photographic film and (b) the autoradiograph. The structure and radiographic image are not in register; the offset was caused by slippage of the film during development. The large oxide patch on the left (a) appears as a continuous dark area in the structure, but the detail within this area can be resolved in the autoradiograph (b). The light areas within these patches are the microvoids described. The dark oxide agglomerate on the right of (a) has no counterpart in (b). Since the autoradiograph cannot distinguish between nonradioactive oxide and a void area, a region such as this cannot be positively identified at present; however, failure to identify this area as a void either with bright-field or polarized illumination suggests that the area represents an oxide patch generated during bonding. Results of electron-microscope surveys of weld areas in aluminum may resolve this question.

IV. CHARACTERIZATION OF WELDMENTS BY ELECTRON MICROSCOPY

A. Background to Electron Microscopy

Electron microscopy is successful in revealing extremely fine particles because electrons are used to illuminate the object instead of light as in the metallurgical microscope. The size of the particle that may be resolved in the light microscope is proportional to the wavelength of the light used to illuminate the particle; that is, the shorter the wavelength of the illuminating beam, the smaller the particles that can be resolved. Physical theory has shown that rapidly propelled electrons may also be considered to have a definite wavelength. This wavelength is variable, being shorter for the higher velocity of the electrons.

These principles form the basis for the high resolution obtainable with the electron microscope. As an example, the wavelength normally used in the electron microscope is of a very small magnitude. Electrons accelerated by a potential difference of 100 kv, behave as though they had a wavelength of 0.04 Å. In contrast to this, the visible radiation generally used with the optical microscope has a wavelength of 4000 to 5000 Å. Thus, the combined short wavelength and high magnification obtainable, up to 200,000 diameters, provide the electron microscope with a resolving power down to 20 Å (0.002μ). In the most modern optical microscope a resolution of only about 2000 Å (0.2μ) is attainable.

B. Reasons for Study

Optical microscopy has been efficiently utilized to characterize ultrasonic weldments. Metallurgical phenomena such as recrystallization, diffusion, and cold work effects, have been readily observed and catalogued. Although such effects are discernible with the optical microscope, their observation is difficult, and sometimes impossible, in monometal weld systems. This restriction coupled with limited resolving power circumscribes the use of optical microscopy.

Electron microscopy is necessary to sufficiently augment study of interfacial mechanics and metallurgy of ultrasonic weldments. With increased magnification and resolving power, weld interface detail is observable and can be interpreted and correlated with previously accumulated ultrasonic weld knowledge. Such a study provides an insight into the mechanism of ultrasonic welding.

C. Experimental Technique

The negative plastic replica technique is the most popular method for preparing samples for electron microscopic observation. The technique lacks, however, in two respects: (1) it is an inverse representation of the original specimen surface contour, and (2) the metal deposit

used to shadow and emphasize the surface detail (so as to enhance contrast and resolution). highlights those areas of the replica which correspond to pits and valleys of the original surface.

Positive replicas, on the other hand, provide a contour-true representation of the specimen surface. This is desirable, for instance, in studying the fine-scale microstructure in ultrasonic weldments of those areas which stand in relief on the original surface. In such cases, a positive replica may be employed which, when shadowed, will highlight ridges and elevations.

Positive replicas also have other attendant advantages. The original specimen surface need not be destroyed by dissolution as would be required if a distortion-free, strain-free negative replica were desired. Thus, the original specimen is available for additional work by other replica methods if the need arises for further confirmatory work. Furthermore, positive replicas can, in general, be made thinner than negative replicas. This is an advantage which is required to obtain efficient electron transmission at high potentials and high magnifications.

A schematic representation of the positive replica technique, used in this electron microscope study for the reasons described, is given in Figure 22. A thick first replica was made with a plastic which was separated from the sample by gentle tapping. The positive replica was then prepared by depositing a thin film of silica normal to the plastic surface. After separation from the plastic, the positive replica was shadowed with chromium metal.

Electron microscopic observations were made on two types of ultrasonically welded monometal samples, Armco iron and commercially pure copper. These metals were prepared for examination by two different techniques. Two 0.032-in. thick iron samples were welded with 2000-watt power, 250-lb clamping force, and 1.5-sec weld time. The 0.032-in. thick copper sheets were welded with 1700-watt power, 600-lb clamping force, and 1.0-sec weld time. One of the duplicate samples was polished and etched by standard metallographic techniques, whereas the companion sample was notched across the top of the weld tab through the weld zone, cooled to -40°F in acetone and dry ice, and fractured while at this low temperature. Positive replicas were then made of the freshly-fractured interfaces and of the metallographically polished samples. These replicas constituted the samples studied with the electron microscope.

D. Discussion of Results

A preliminary study of the electron micrographs obtained to date on welded iron and copper samples revealed some interesting facets concerning the character of the weldment interface. The most striking feature was the violent interface deformation shown in Figure 23. In Figure 24, the polished and etched iron, contrast on opposite sides of the weldment is visible as a difference in etching detail.

The metal at the interface appears to be moved in a swirling pattern, a movement that could be correlatable with photoelastic observations made and reported in Progress Report 4. The swirling action of the metal interface during ultrasonic welding can be visualized when viewing the wrinkled areas in the copper weld and interpenetration of the iron faying surfaces that are visible in Figure 24.

No evidence of melting at the weldment interfaces of iron and copper monowelds has been uncovered to date. Although breadth of the interface was observed, fine structural details within the interface bond denoting melting were not observed.

Table I

TENSILE-SHEAR STRENGTH DATA
FROM LATIN SQUARE DESIGN EXPERIMENT
ON ALUMINUM OXIDE FILM* IMPREGNATED
0.0335-INCH HIGH-PURITY ALUMINUM

Mean ± 90% Confidence Interval
Time: 1-1/2 sec, constant

	Oxide Thickness Level, Å					
	500		1000		3000	
Power, watts	CF, lb*	T-S, lb/spot#	CF, lb*	T-S, lb/spot#	CF, lb*	T-S, lb/spot#
1000	600	420 ± 30	400	410 ± 20	500	440 ± 30
1300	500	455 ± 20	600	450 ± 20	400	440 ± 10
1600	400	450 ± 20	500	455 ± 10	600	480 ± 10

* Clamping Force.
\# Tensile-Shear Strength.

Table II

ANALYSIS OF VARIANCE FOR THE EXPERIMENTAL DATA PRESENTED IN TABLE I

Source of Variation	df	Sum of Squares	Mean Squares	F	Significance
Power, watts	2	6548.032	3274.016	28.32	P 99.9%
Oxide Coating, Å	2	1003.328	501.664	4.34	P 95%
Clamping Force, lb	2	1706.453	853.226	7.38	P [illegible]7%
Replicates	2	228.588	114.294	0.99	
Experimental Error	18	2078.993	115.4996		
Total	26	11,565.394			

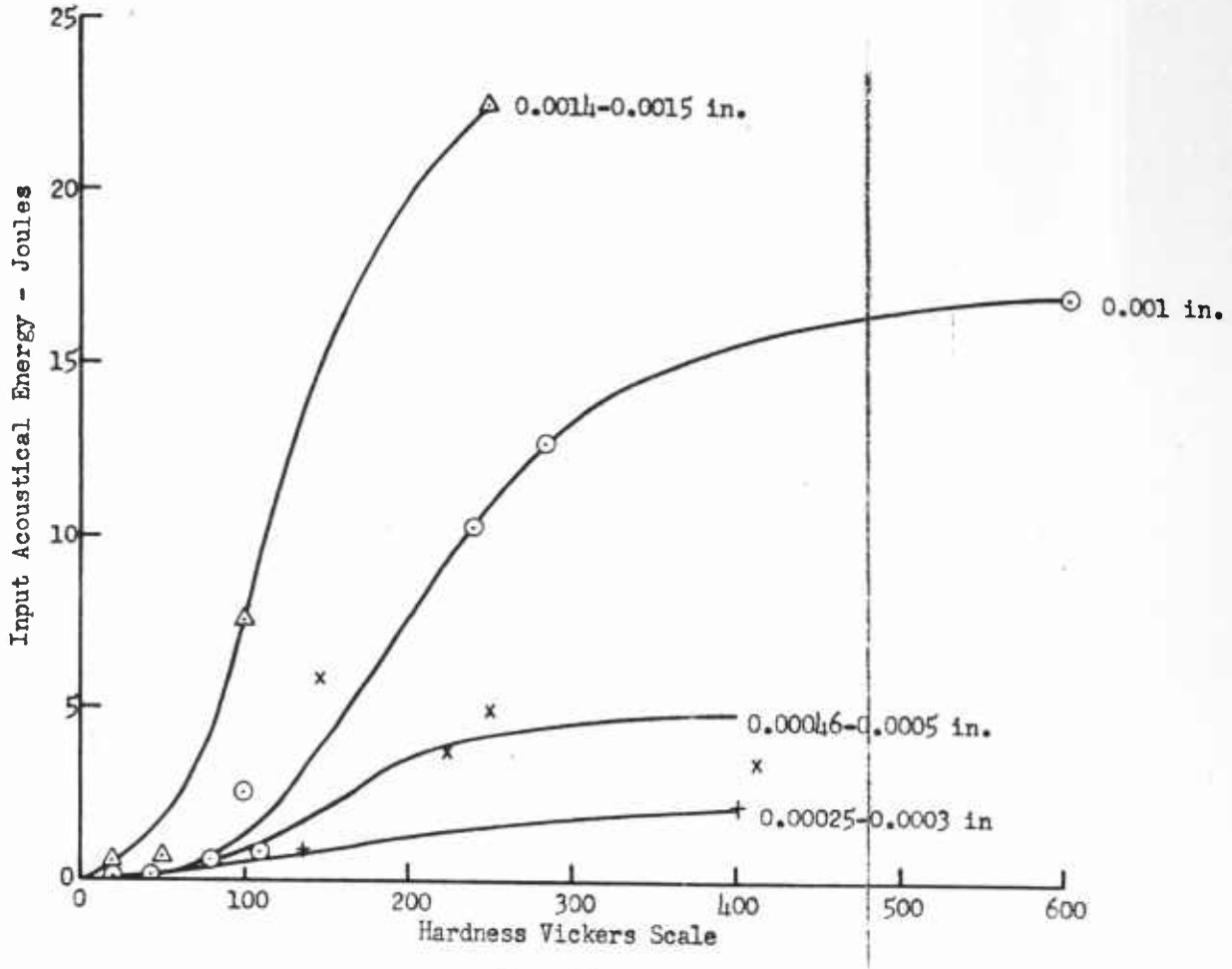

Figure 1

ACOUSTICAL ENERGY REQUIRED TO GENERATE A WELD AS A FUNCTION OF HARDNESS WITH PARAMETER OF MATERIAL THICKNESS

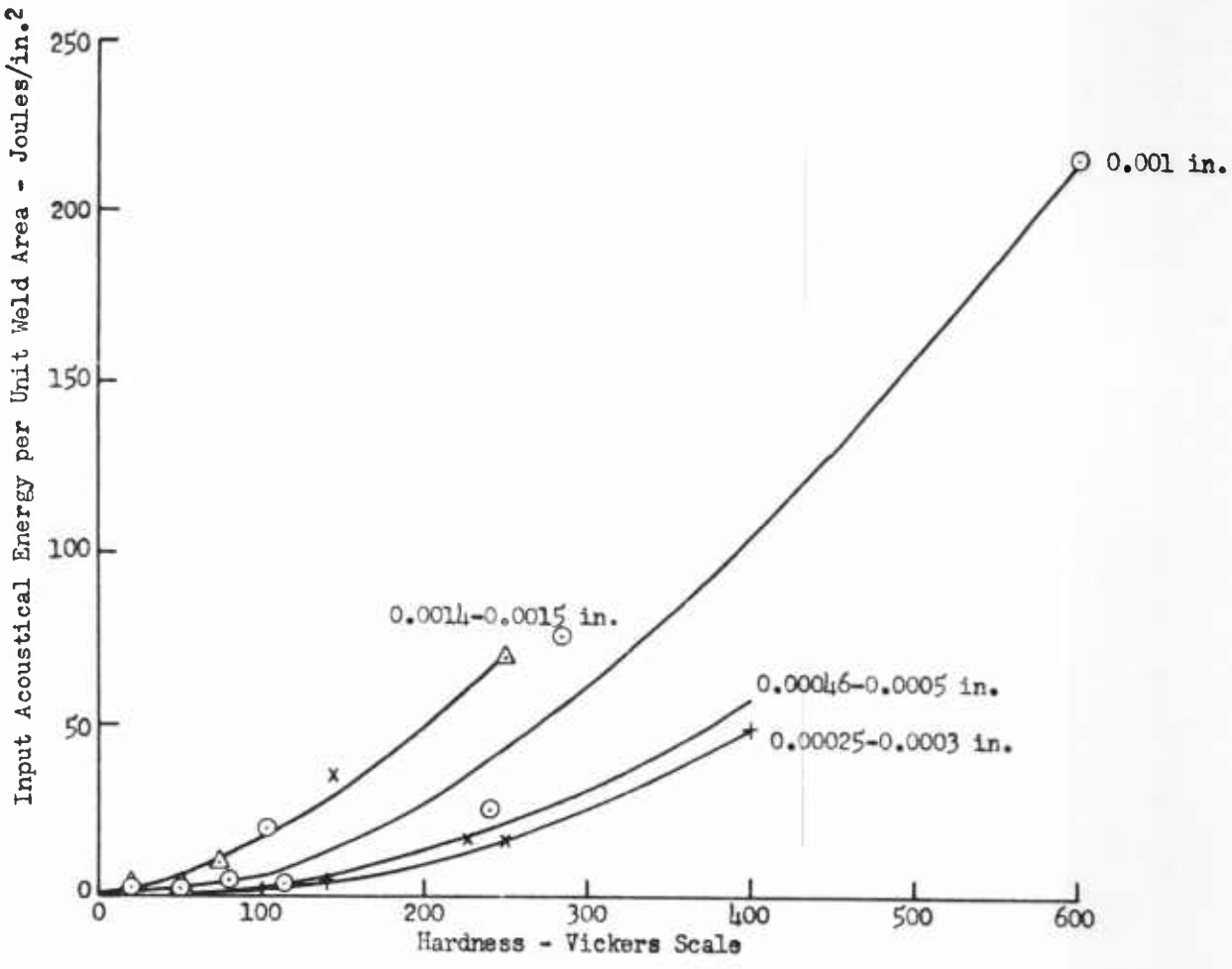

Figure 2

ACOUSTICAL ENERGY REQUIRED TO GENERATE A WELD AS A FUNCTION OF HARDNESS WITH PARAMETER OF MATERIAL THICKNESS

Figure 3

ACOUSTICAL ENERGY REQUIRED TO GENERATE A WELD AS A FUNCTION OF MATERIAL THICKNESS WITH PARAMETER OF VICKERS HARDNESS

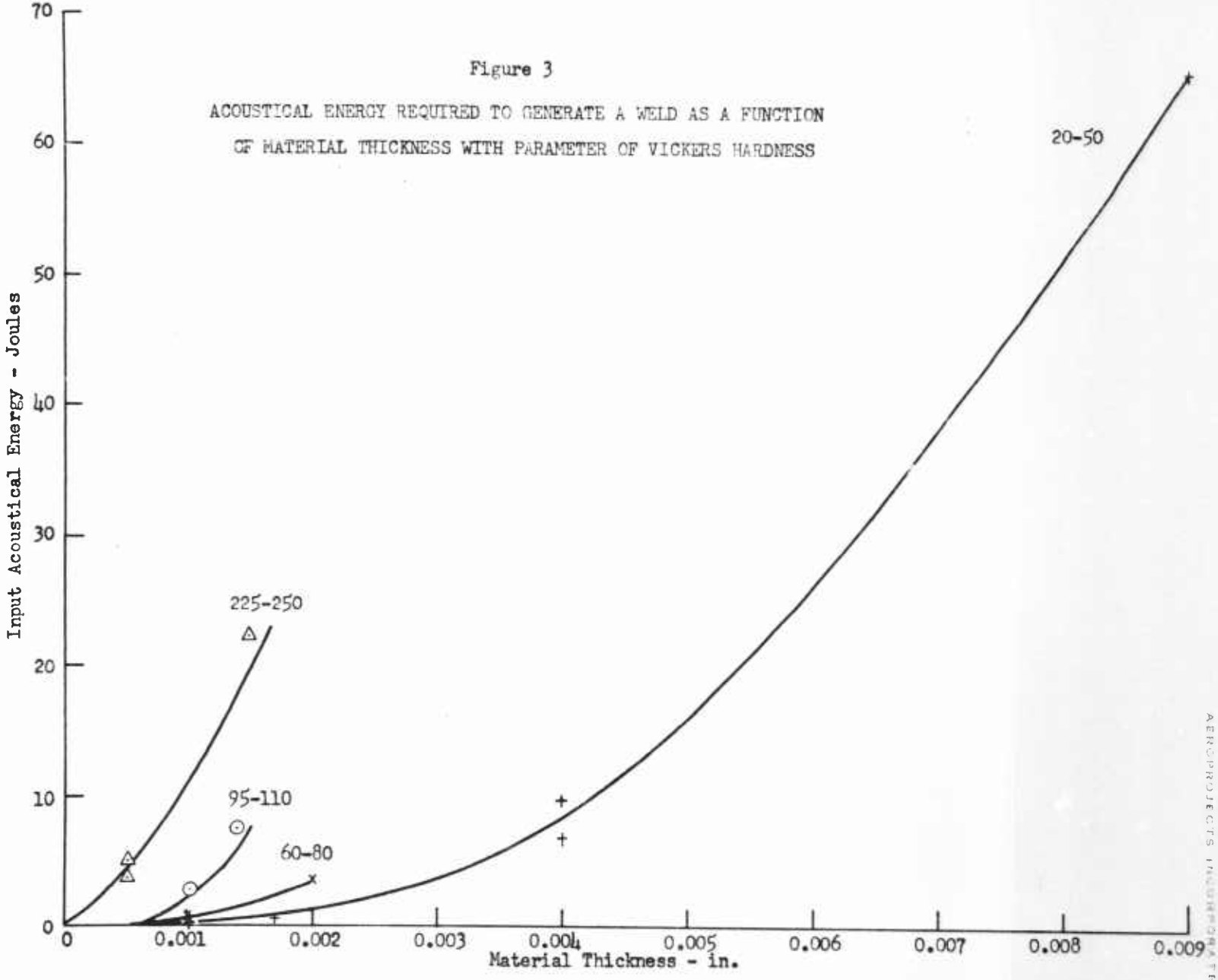

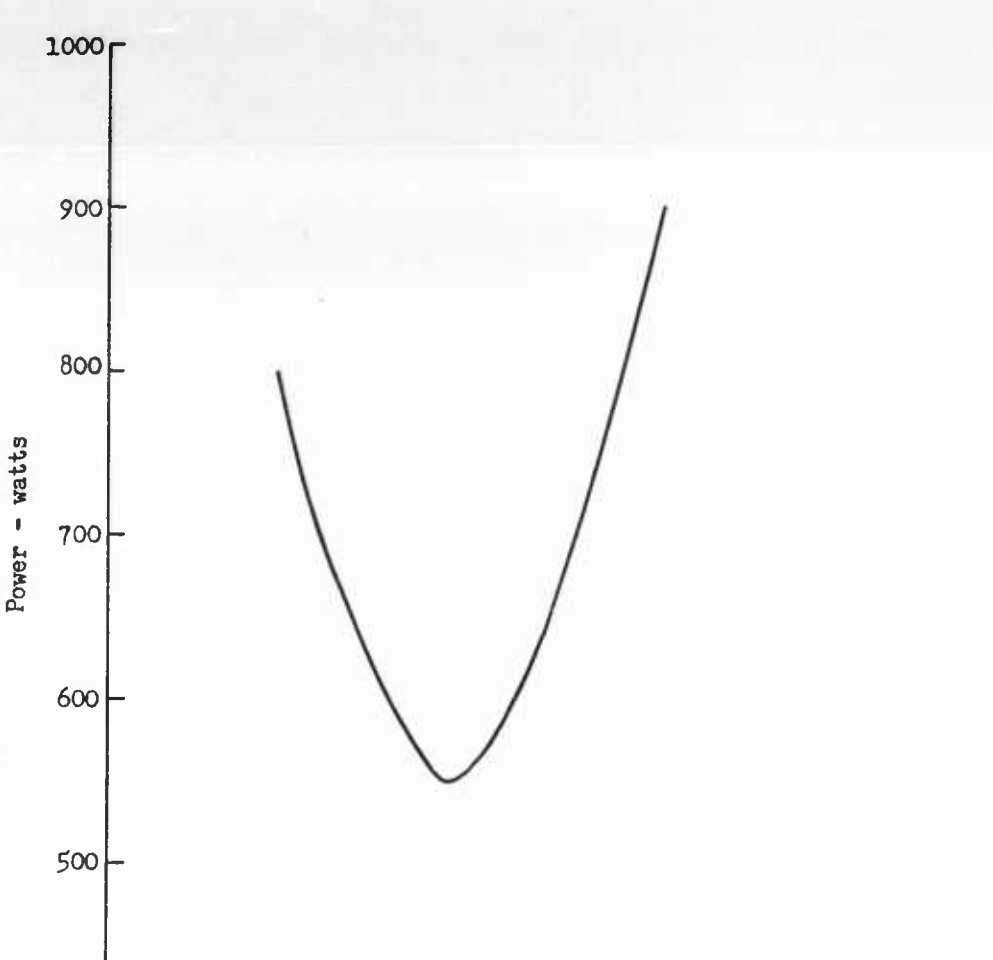

Figure 4

THRESHOLD CURVE FOR NUGGET PULLOUT WELDS
ON 0.005-IN. HALF-HARD COPPER

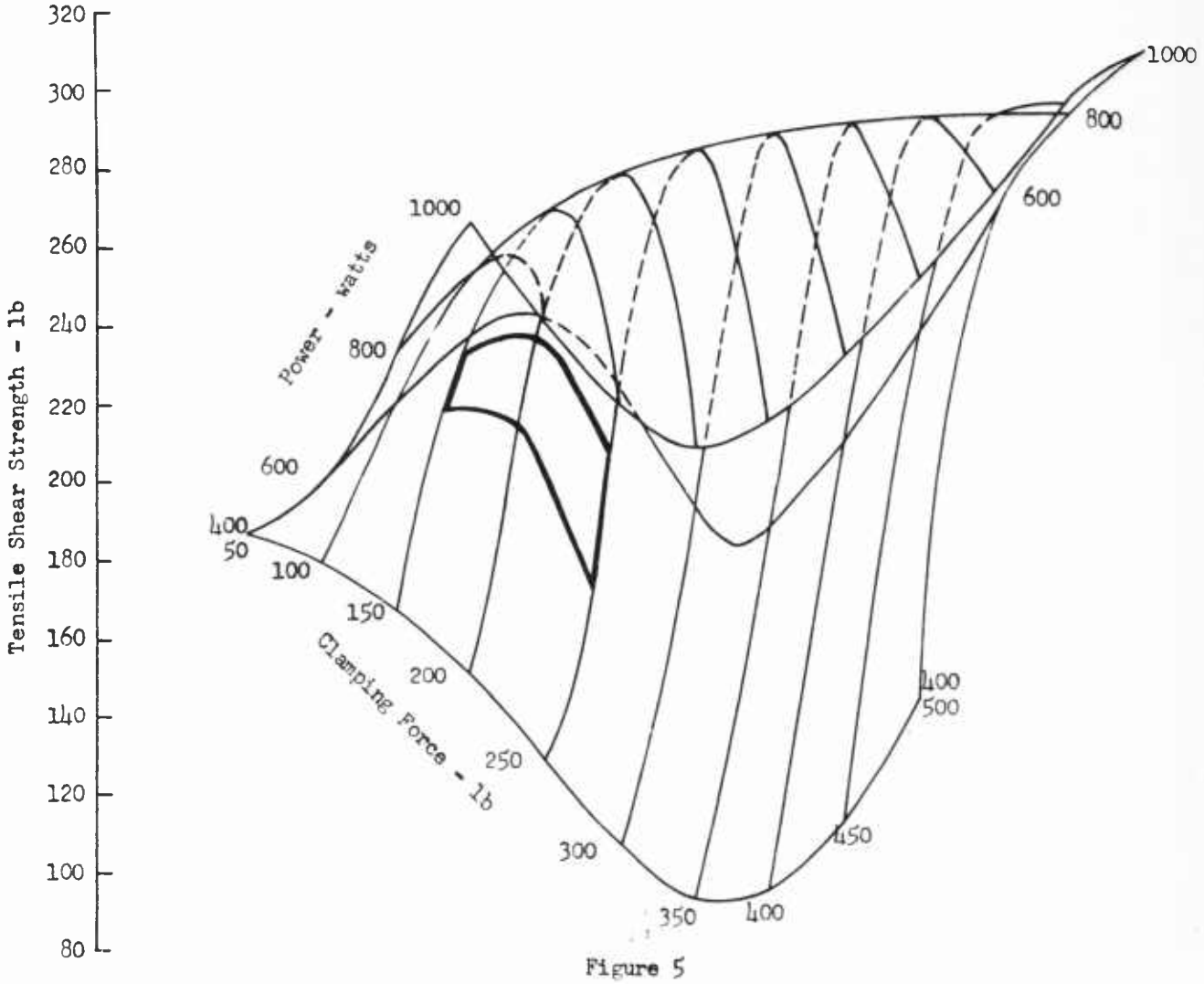

Figure 5

EFFECT OF CLAMPING FORCE AND POWER ON TENSILE SHEAR STRENGTH OF A WELD ON 0.005-IN. 302 STAINLESS STEEL

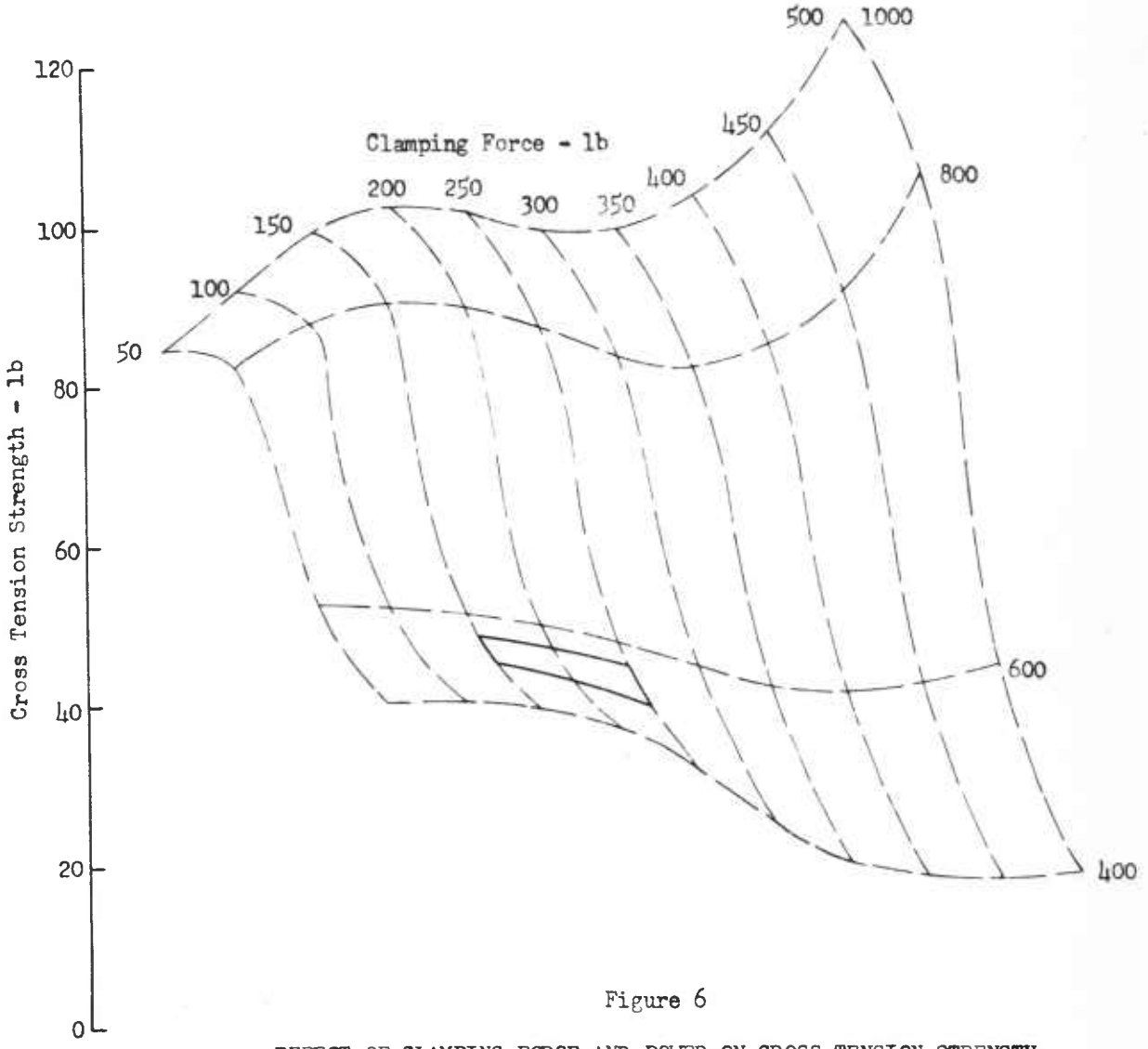

Figure 6

EFFECT OF CLAMPING FORCE AND POWER ON CROSS TENSION STRENGTH OF A WELD ON 0.005-IN. 302 STAINLESS STEEL

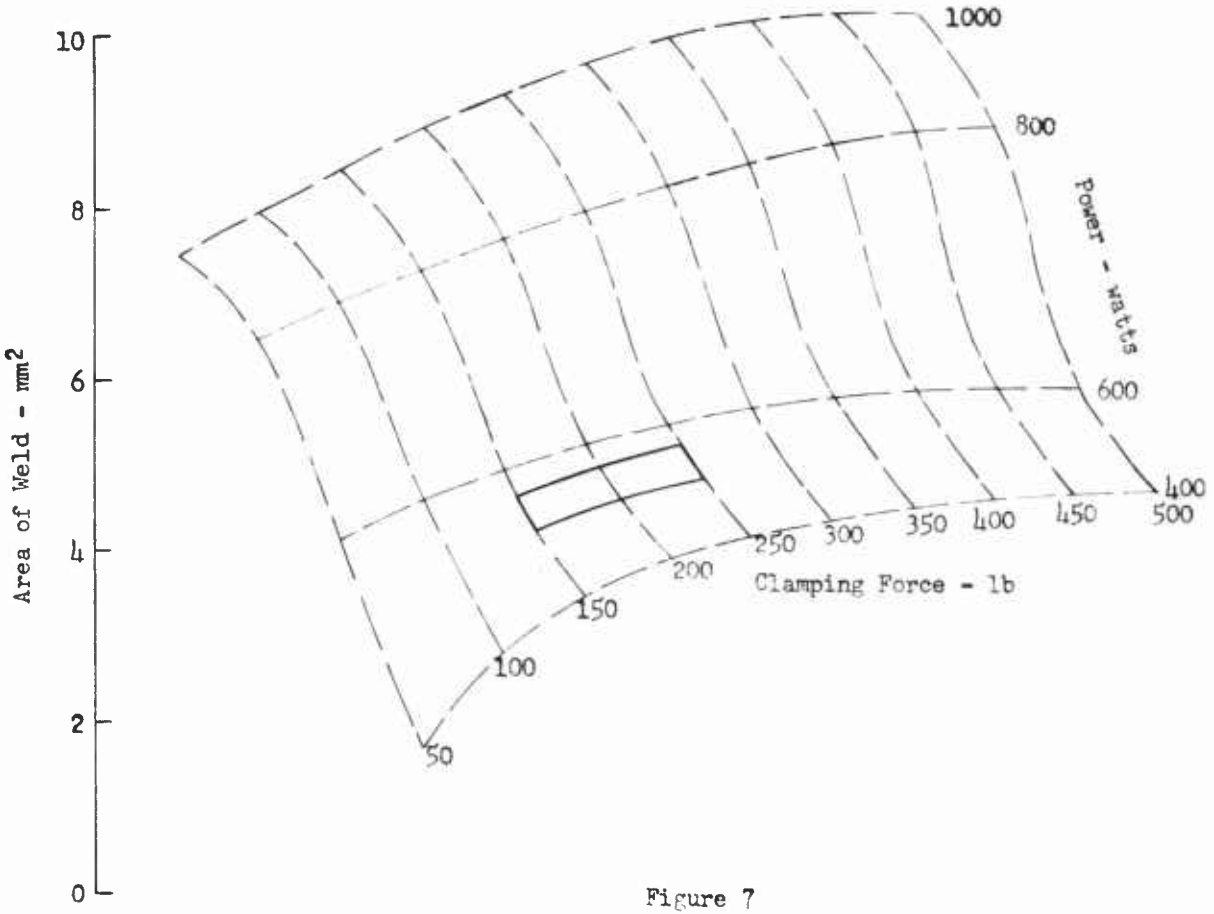

Figure 7

EFFECT OF CLAMPING FORCE AND POWER ON WELD AREAS
ON 0.005-IN. COLD ROLLED 302 STAINLESS STEEL

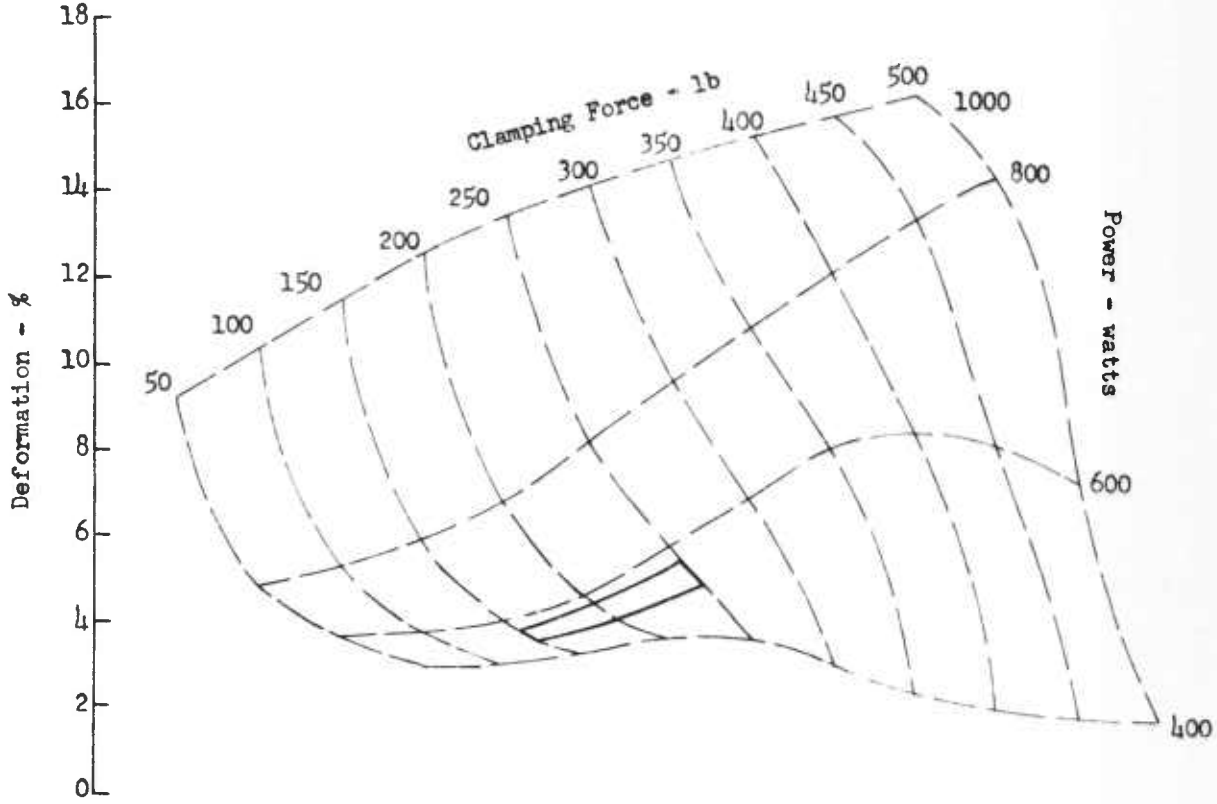

Figure 8

EFFECT OF CLAMPING FORCE AND POWER ON DEFORMATION OF A WELD ON 0.005-IN. STAINLESS STEEL

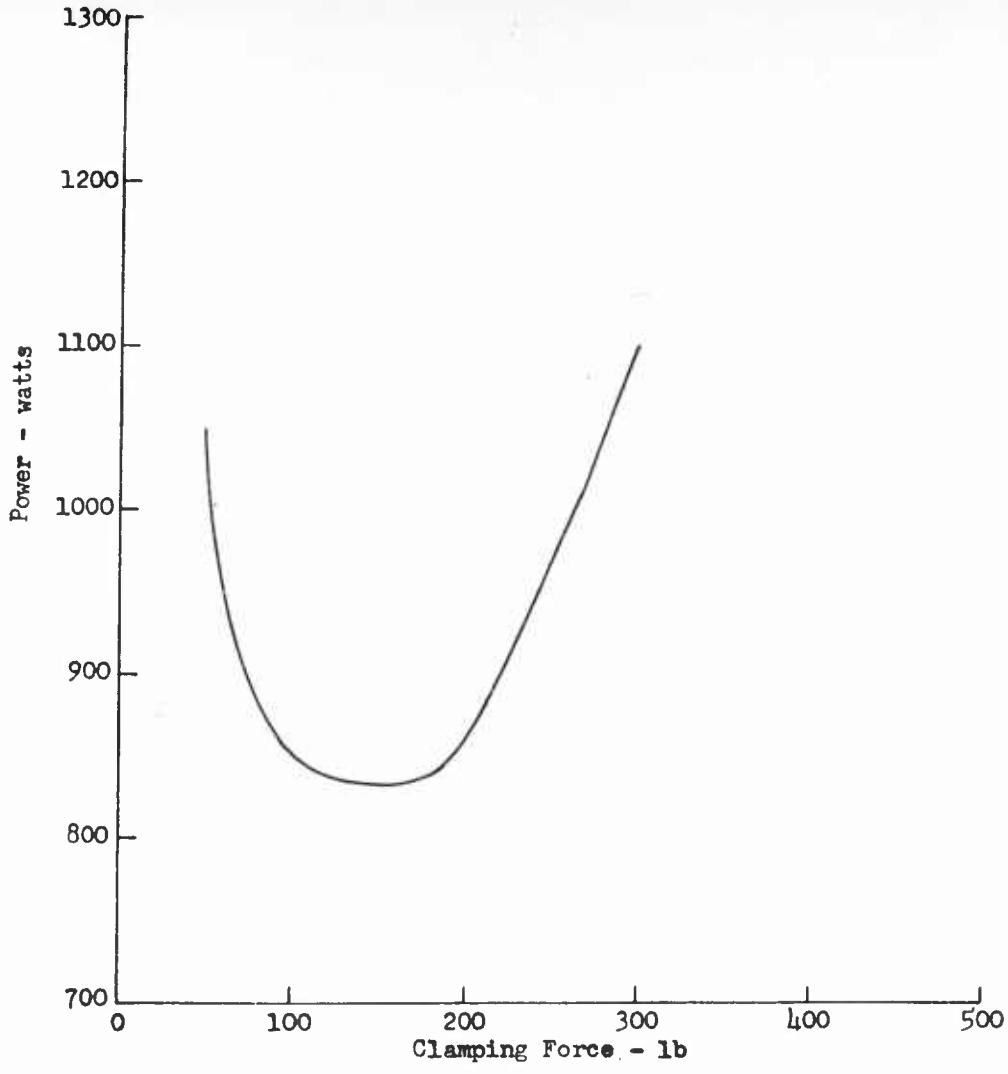

Figure 9

THRESHOLD CURVE FOR NUGGET PULLOUT WELDS
ON 0.010-IN. ANNEALED 302 STAINLESS STEEL

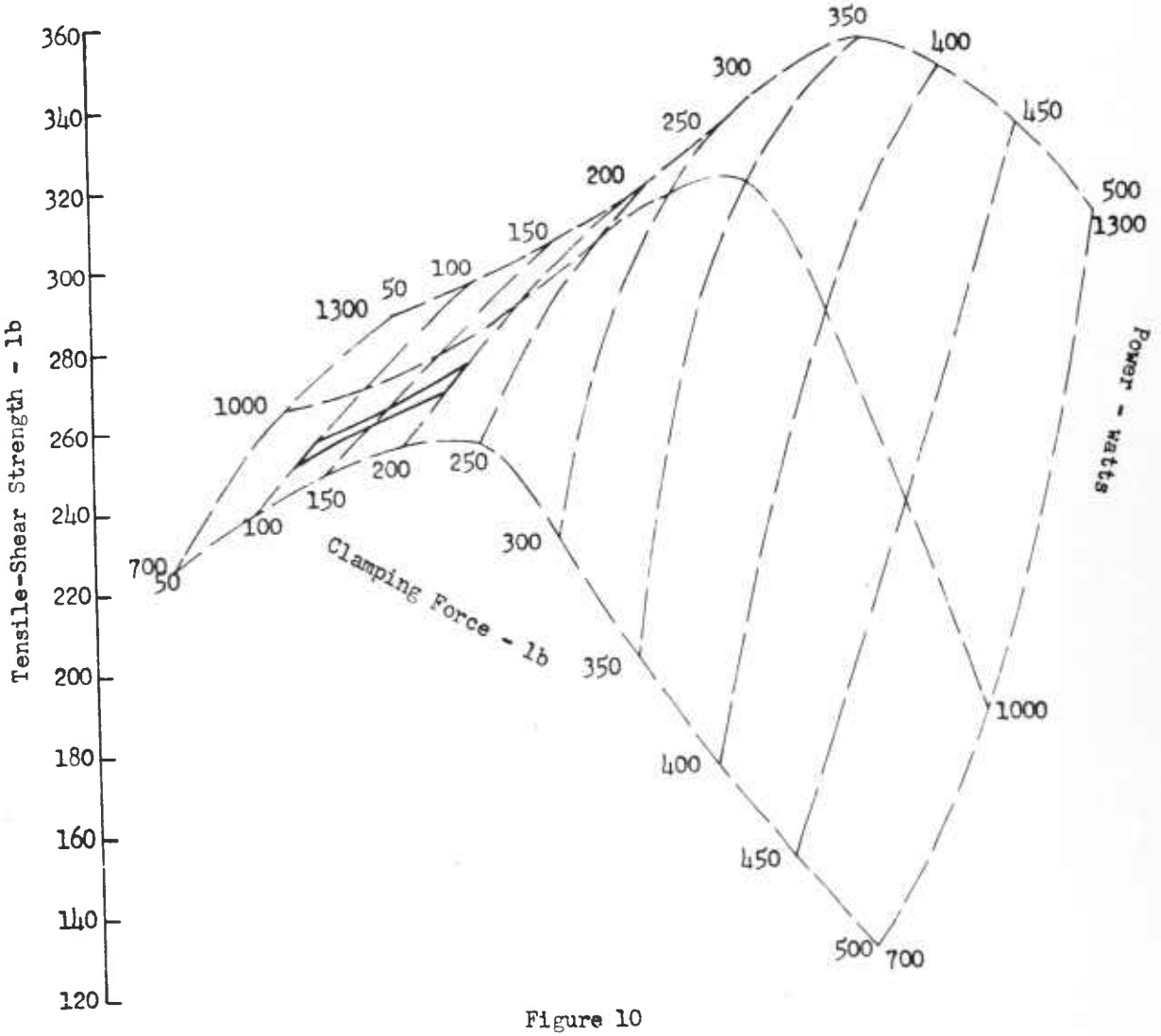

Figure 10

EFFECT OF CLAMPING FORCE AND POWER ON TENSILE-SHEAR STRENGTH OF A WELD ON 0.010-IN. STAINLESS STEEL

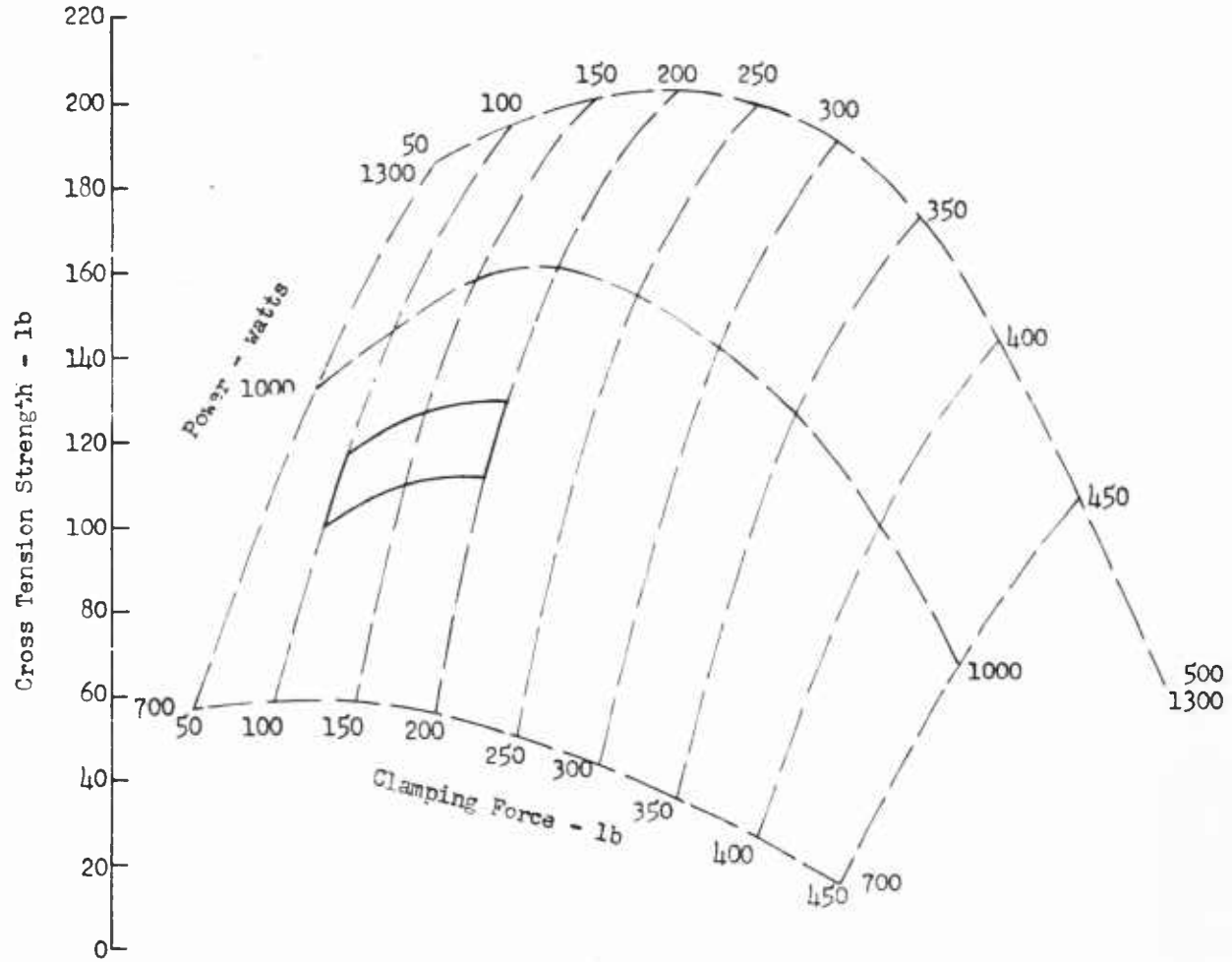

Figure 11

EFFECT OF CLAMPING FORCE AND POWER ON CROSS TENSION STRENGTH OF A WELD ON 0.010-IN. 302 STAINLESS STEEL

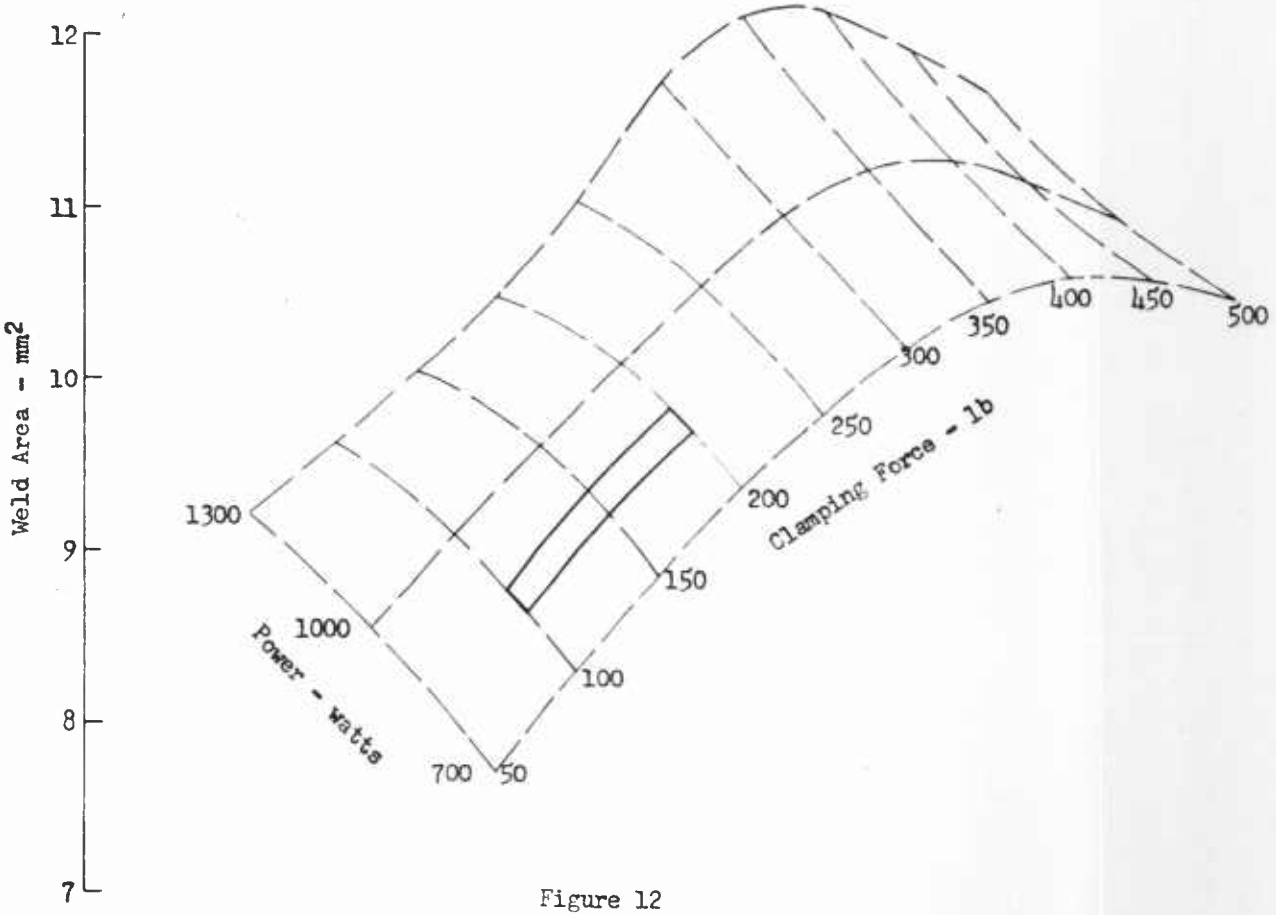

Figure 12

EFFECT OF CLAMPING FORCE AND POWER
ON WELD AREAS ON 0.010-IN. 302 STAINLESS STEEL

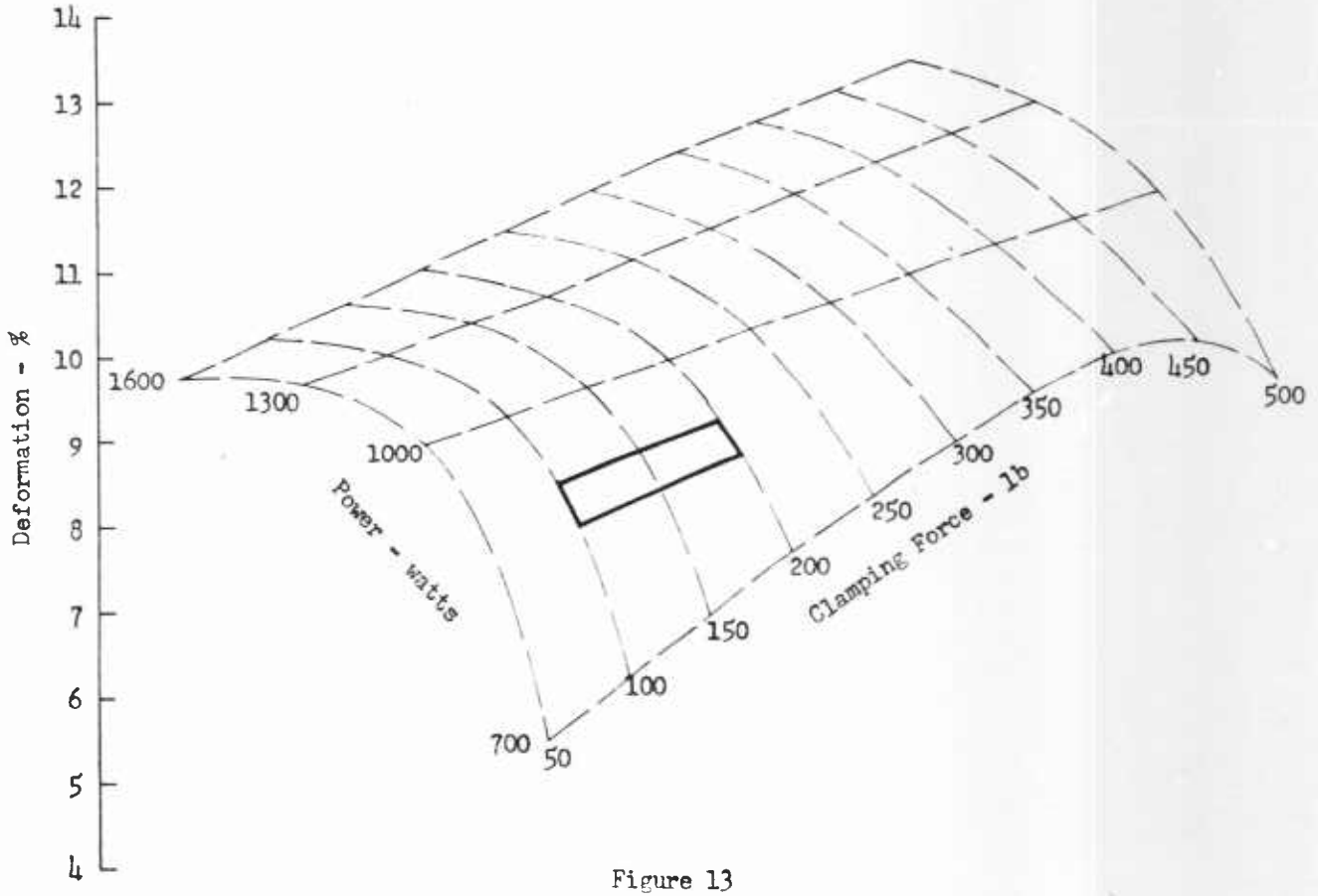

Figure 13

EFFECTS OF CLAMPING FORCE AND POWER ON DEFORMATION OF A WELD ON 0.010 IN. ANNEALED 302 STAINLESS STEEL

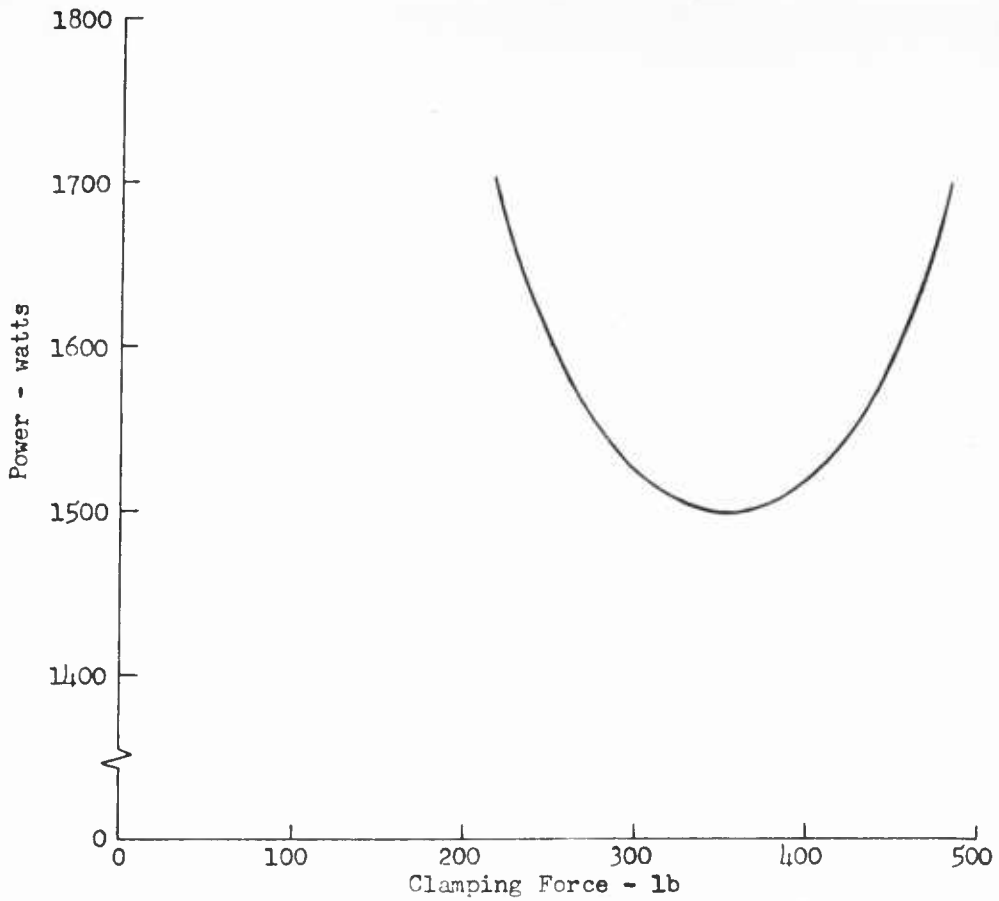

Figure 14

THRESHOLD CURVE FOR NUGGET PULLOUT WELDS
ON 0.020-IN. HALF-HARD COPPER

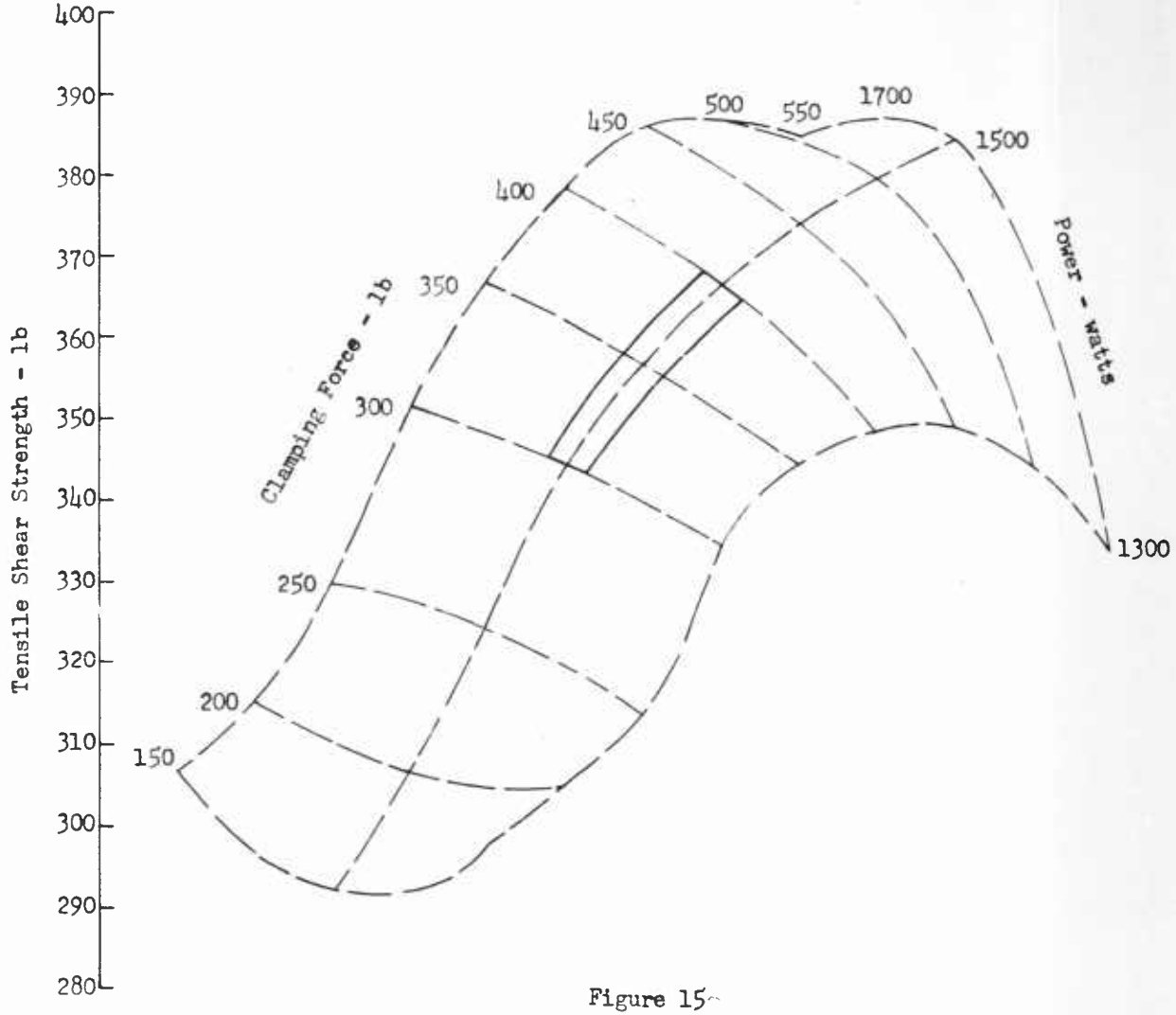

Figure 15

EFFECT OF CLAMPING FORCE AND POWER ON TENSILE-SHEAR STRENGTH OF A WELD ON 0.020-IN. HALF-HARD COPPER

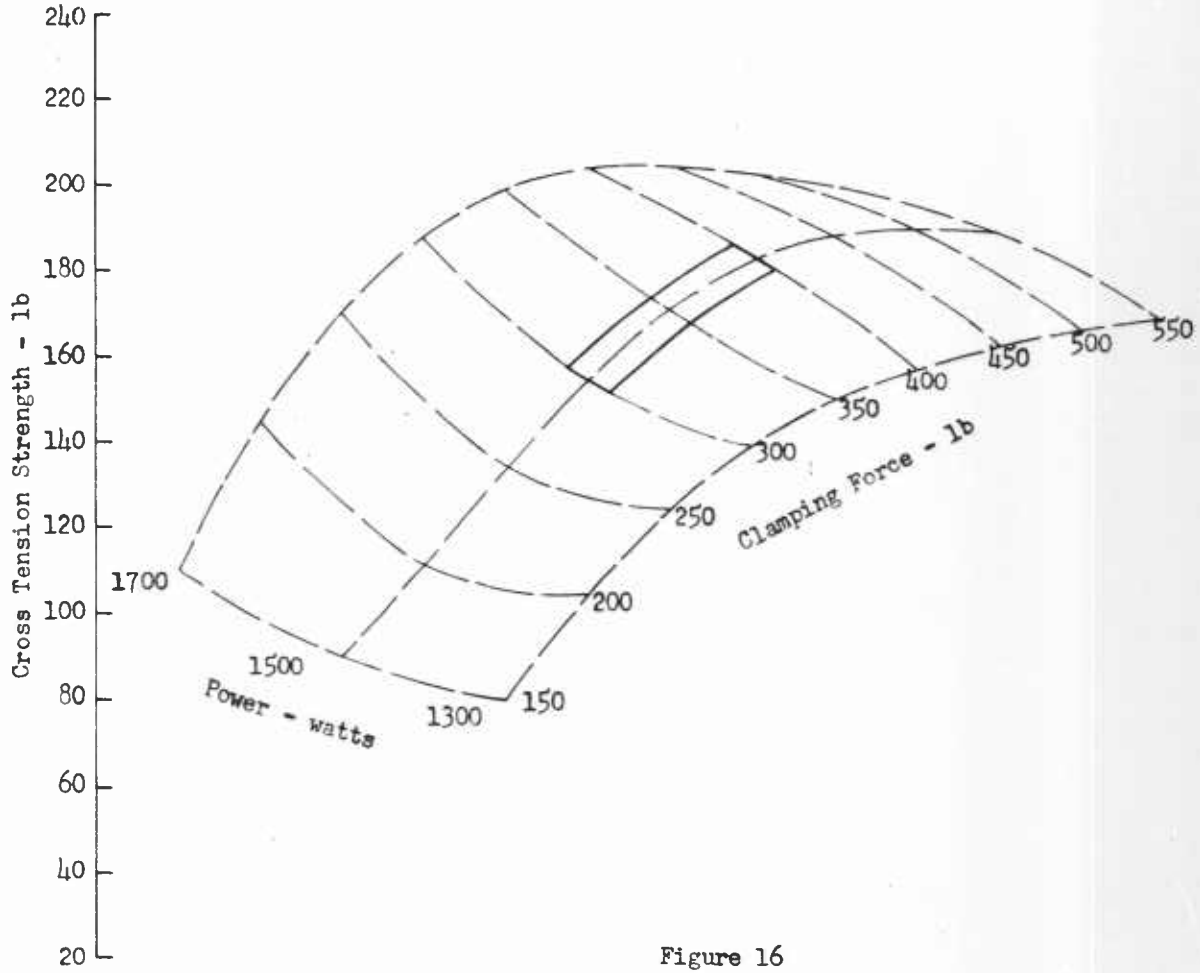

Figure 16

EFFECT OF CLAMPING FORCE AND POWER ON CROSS-TENSION STRENGTH OF A WELD ON 0.020-IN. HALF-HARD COPPER

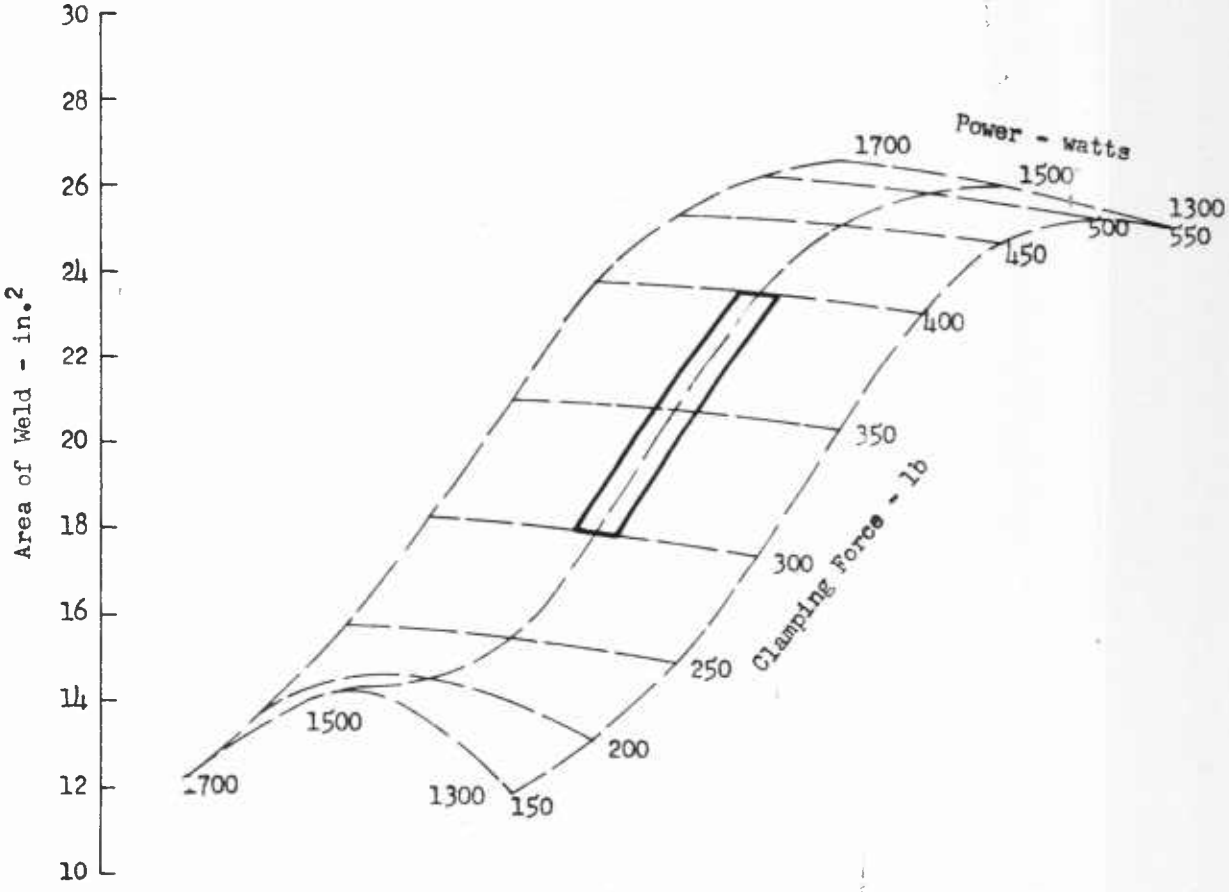

Figure 17

EFFECT OF CLAMPING FORCE AND POWER
ON WELD AREAS ON 0.020-IN. HALF-HARD COPPER

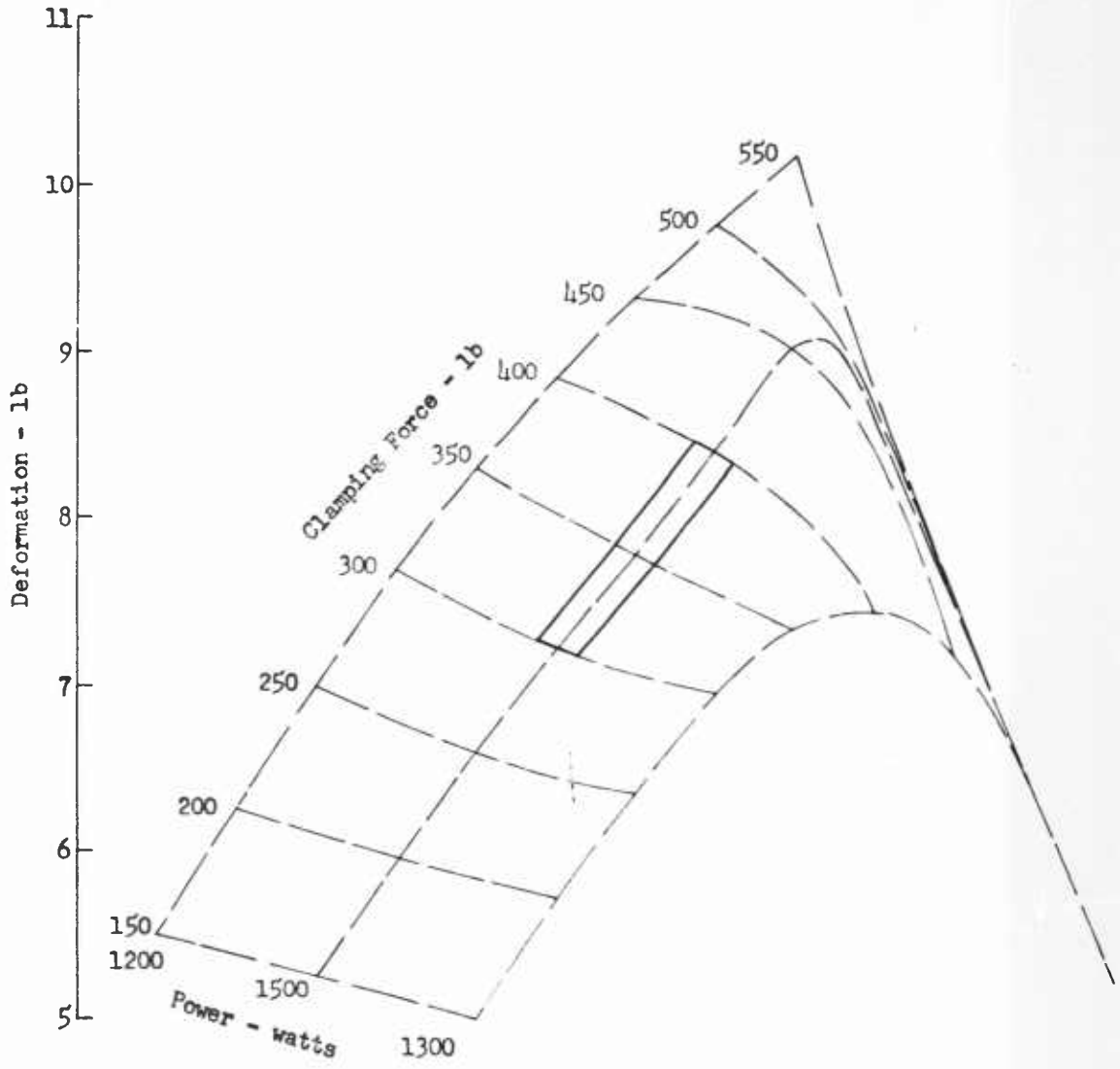

Figure 18

EFFECT OF CLAMPING FORCE AND POWER ON DEFORMATION OF A WELD ON 0.020-IN. HALF-HARD COPPER

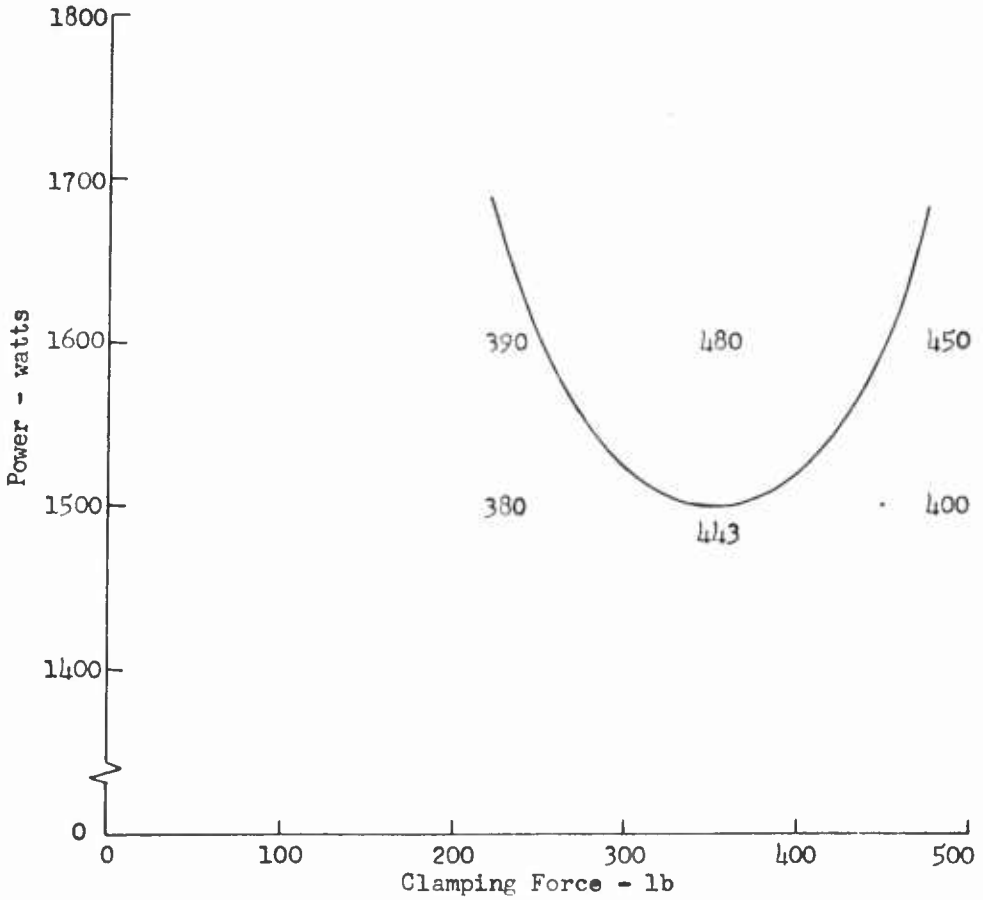

Figure 19

THRESHOLD CURVE WITH TYPICAL TEMPERATURES (°F) NOTED AT INTERFACE FOR VARIOUS POWER AND CLAMPING FORCE LEVELS FOR 0.020 IN. HALF-HARD OFHC COPPER

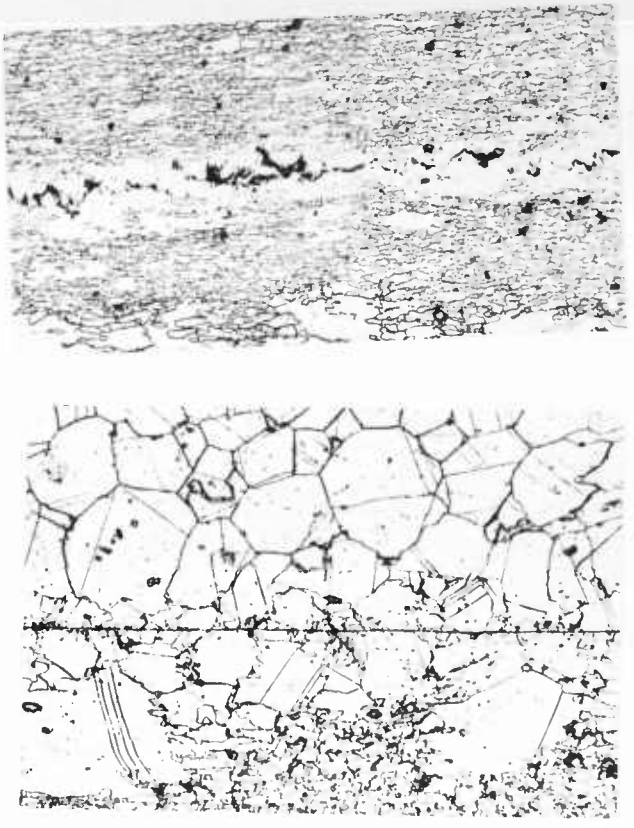

(a)

(b)

Figure 20

ULTRASONIC WELDS IN 0.012-INCH INCONEL X
IN THE SOLUTION HEAT TREATED CONDITION

Specimen (a) was bonded without removing heat-treat scale; (b) was chemically deoxidized.

Oxalic acid etch (electrolytic), 150X

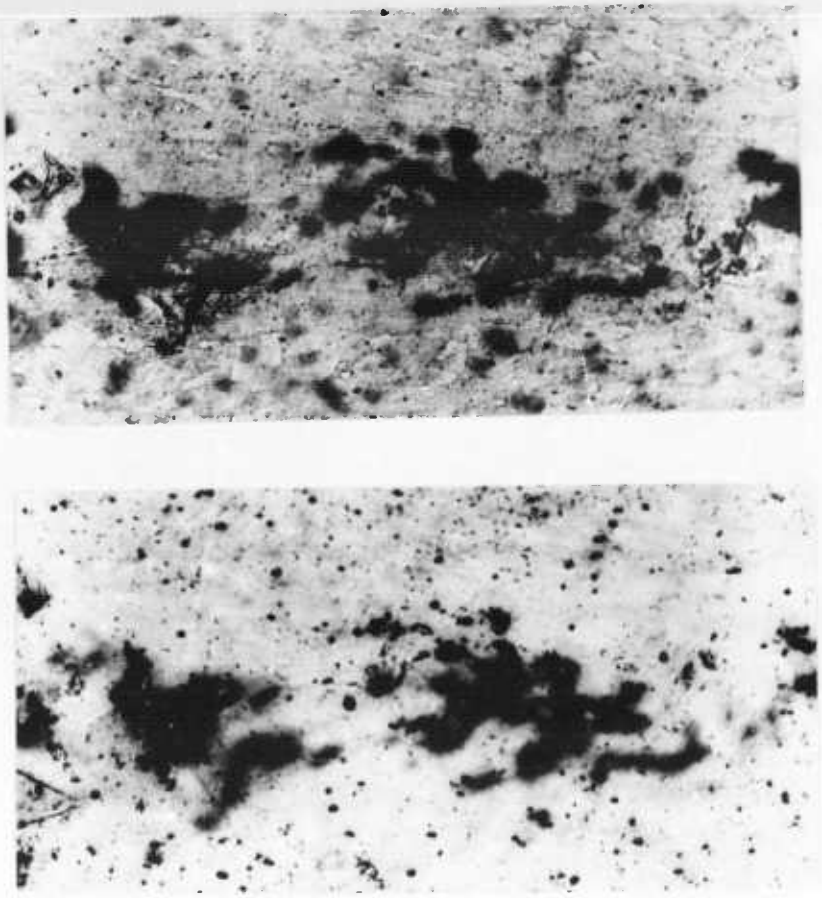

(a)

(b)

Figure 21

PHOTOMICROGRAPH OF STRUCTURE (a) AND AUTORADIOGRAPH (b)
OF SAME INTERFACIAL AREA OF ULTRASONIC WELD IN ANODIZED (3000 A) ALUMINUM
0.5% HF etch, 500X

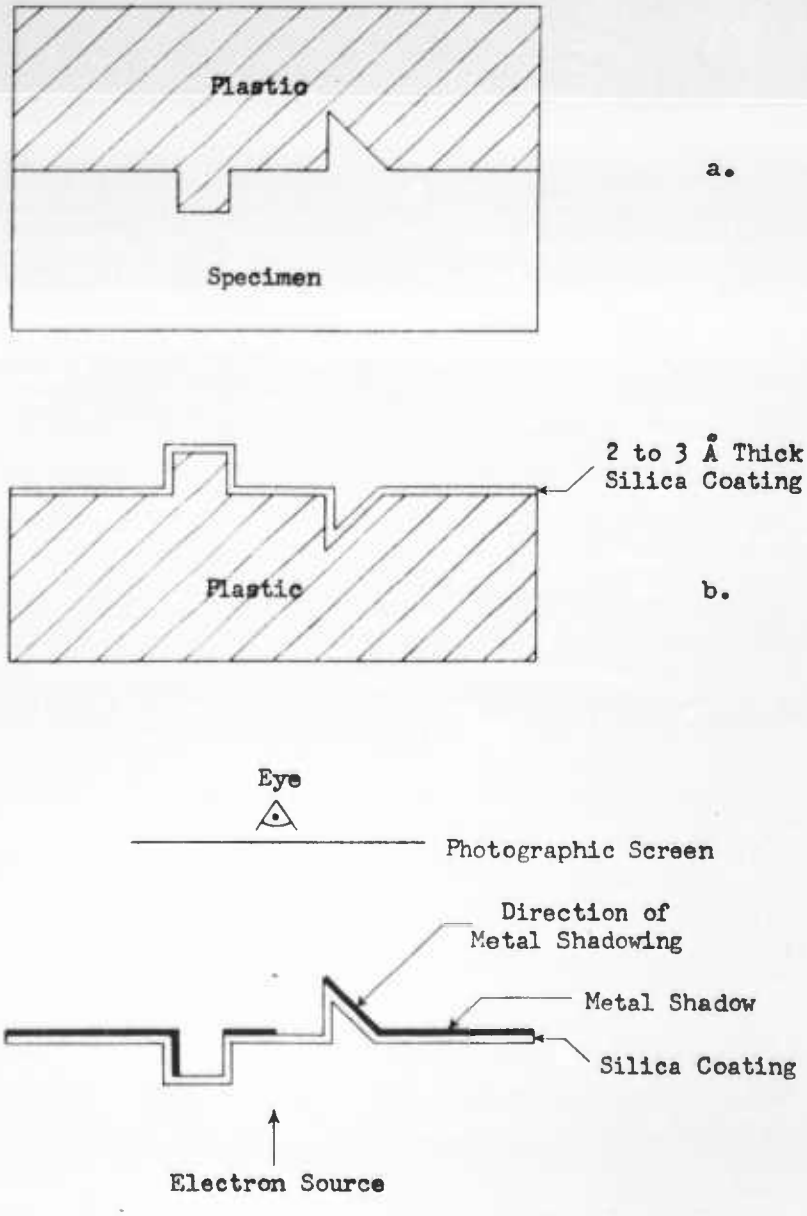

Figure 22

SCHEMATIC REPRESENTATION OF CROSS SECTION
OF POSITIVE SHADOWED REPLICA

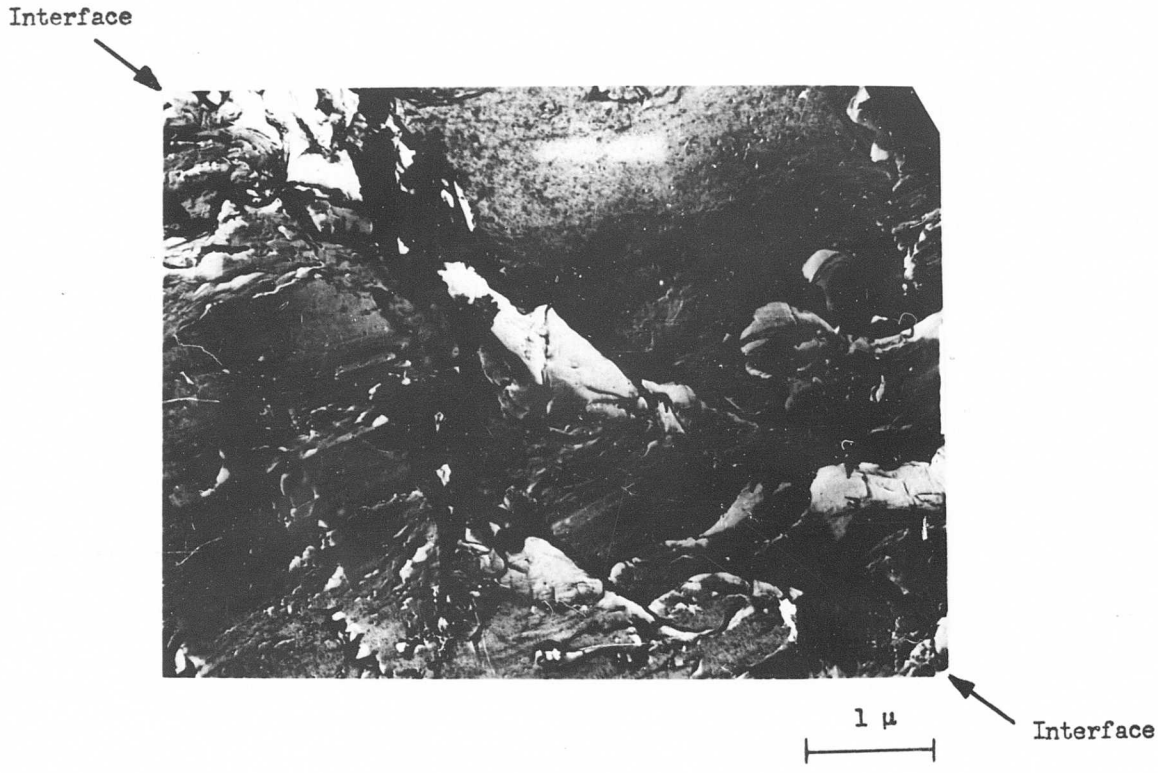

Figure 23

ELECTRON FRACTOGRAPH OF ULTRASONICALLY WELDED
CHEMICALLY PURE COPPER
(Positive shadowed silica replica)
Note the swirling pattern of deformation at the interface.
Magnification: 20,000X

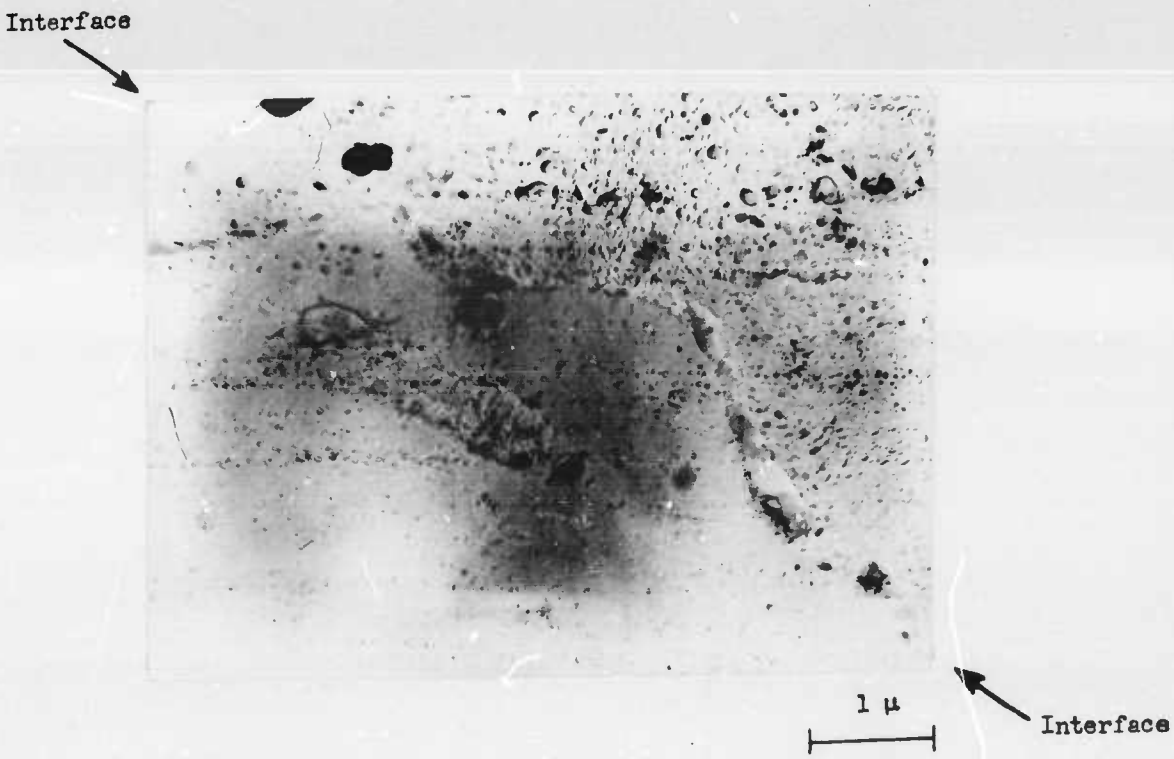

Figure 24

ELECTRON MICROGRAPH OF ULTRASONICALLY WELDED ARMCO IRON

Longitudinal section through weld spot welded with 2000-electrical watts at 250-lb clamping force for 1.5 sec was polished and etched by standard metallographic techniques. Positive shadowed silica replica. Note the interpenetration below the interface and the greater etching detail on the upper right-hand side of the weldment.

Magnification: 20,000X